CONTENTS

	Page	
INTRODUCTION AND SUMMARY	1	1/A7
MATHEMATICAL REPRESENTATION OF A POISSON PROCESS	2	1/A8
DERIVATION OF OPTIMUM ESTIMATORS	6	1/A12
OPTIMUM AND SUBOPTIMUM ESTIMATOR PERFORMANCE	19	1/B11
PERFORMANCE OF SUBOPTIMUM RECEIVER STRATEGIES	29	1/C7
CONCLUSIONS AND AREAS FOR FUTURE STUDY	33	1/C11
ACKNOWLEDGMENTS	35	1/C13
REFERENCES	37	1/D1

NAS 1.60:1315

SEP 25 NASA

NASA Technical Paper 1315

COMPLETED
ORIGINAL

A Comparative Study of Optimum and Suboptimum Direct-Detection Laser Ranging Receivers

James B. Abshire

SEPTEMBER 1978

NASA

44

NAS 1.60:1315

NASA Technical Paper 1315

A Comparative Study of Optimum and Suboptimum Direct-Detection Laser Ranging Receivers

James B. Abshire
Goddard Space Flight Center
Greenbelt, Maryland

National Aeronautics
and Space Administration

**Scientific and Technical
Information Office**

1978

All measurement values are expressed in the International System of Units (SI) in accordance with NASA Policy Directive 2220.4, paragraph 4.

ABSTRACT

A summary of previously proposed receiver strategies for direct-detection laser ranging receivers is presented. Computer simulations are used to compare performance of candidate implementation strategies in the 1- to 100-photoelectron region. Under the condition of no background radiation, the maximum-likelihood (ML) and minimum mean-square error (MMSE) estimators were found to give the same performance for both bell-shaped and rectangular optical-pulse shapes. For signal energies greater than 10 photoelectrons, the root-mean-square (rms) range error is shown to decrease as $Q^{-1/2}$ for bell-shaped pulses and Q^{-1} for rectangular pulses, where Q represents the average pulse energy. Of several receiver implementations presented, the matched-filter peak detector was found to be preferable. A similar configuration, using a constant-fraction discriminator, exhibited a signal-level dependent time bias. Suggestions for future study are also included.

Blank PAGE

A COMPARATIVE STUDY OF OPTIMUM AND SUBOPTIMUM DIRECT-DETECTION LASER RANGING RECEIVERS

James B. Abshire
Goddard Space Flight Center
Greenbelt, Maryland

INTRODUCTION AND SUMMARY

Since the development of high-power pulsed lasers, there has been a widespread interest in the application of these devices to optical radar systems. The development of laser ranging systems within the National Aeronautics and Space Administration (NASA), for example, began in the early 1960's and has grown substantially in the intervening years (Reference 1). The application of accurate range measurements to Earth-orbiting satellites has produced important results in precise orbit and gravity-field determinations and is expected to produce in the near future the same unique findings relating to the crustal motions of the Earth. Because the potential usefulness of laser ranging data is directly related to its accuracy, there is considerable interest in developing optimum laser ranging receivers.

Several studies have been made of optical radar receivers. An early study (Reference 2) compared the performance of direct-detection versus heterodyne receivers and found that, for conditions frequently encountered in practice, the direct-detection receiver had superior target detection and ranging performance despite the greater complexity of the heterodyne receiver. The performance of the heterodyne receiver was found to exceed the simpler direct-detection receiver only when background noise was very heavy or when high-velocity resolution was required.

As a result of these findings, several methods have been outlined for implementing the direct-detection receiver when the return optical pulse shape is known in advance (References 3 through 5). In addition, recent work has studied direct-detection receivers for use when the return pulse shape is randomly broadened by the radar target (References 6 and 7)

In this document, the ranging performance of several proposed direct-detection receivers is compared. As necessary background, the minimum mean-square error (MMSE) and maximum-likelihood (ML) estimators for optical pulse delay are derived. These estimators are shown to be equivalent in the special case of the receiver operating with no background illumination and with either bell-shaped or rectangular pulse shapes. The error performance of the ML estimator is derived under the assumption of high optical signal to background

ratios and differentiable optical pulse shapes. The results of computer simulations show the performance of the ML receiver operating under low signal energies and with increasingly rectangular pulse shapes and represent new results in this area. The simulated performance of a modified ML receiver is also presented.

Finally, the ranging performance of optimum and suboptimum receiver configurations is compared, and the results are used to outline possible improvements to current laser-ranging receiver design.

MATHEMATICAL REPRESENTATION OF A POISSON PROCESS

It has been shown that the beam fluctuations, and therefore the photocount, from a single-mode laser beam follow Poisson statistics (Reference 8). Furthermore, when noise is absent, the photocount rate varies as the signal that modulates the beam and, when noise is present, as the signal plus noise.

The noise in laser-ranging receivers is attributable to both detector dark current and background radiation, which are also believed to follow Poisson statistics. In all NASA laser ranging systems that have been planned or built to date, high-gain photomultipliers have been used as detectors. In systems using these detectors, effects of thermal noise on receiver performance are negligible.

For the theoretical model used in this study, the laser transmitter is treated as a photon source whose average output power is modulated by a deterministic waveform $\lambda_s(t)$ of limited time duration. In general, the received data will consist of a series of randomly distributed points in time, t_j, $j = 1,2,\ldots,M$, within the time interval, $(-T, T)$. Here, both the t_j's and the total number of observed photocounts, M, are random variables. The t_j's are a realization of a Poisson point process with time-varying expectation $\lambda(t)$. For the range estimation problem, $\lambda(t) \equiv \lambda_r(t - \tau) + \lambda_n$, where $\lambda_r(t)$ is known and λ_n represents a uniform background noise count rate (attributable to background illumination on the photodetector or internally generated detector noise counts). The time interval, $(-T, T)$, represents the limits on the prior range uncertainty and is assumed to be equal to the observation interval. For the MMSE and ML estimators, it is assumed $\lambda_r(t - \tau) = \lambda_s(t - \tau)$ (that is, the average received optical pulse snape is equal to that of the transmitter). The receiver is required to estimate the time-of-arrival of the optical pulse, τ, given observation of the photocounts, t_j, $j = 1,2,\ldots,M$ within $(-T, T)$.

This simple model of the optical detection process has at least two limitations. First, if the optical pulse was produced by several interacting laser modes or by an incoherent optical source, the photoelectron distribution is not necessarily Poisson (Reference 8). Also, the model assumes that observation of the individual photoelectric emission times at the detector is accurate. In practice, photomultipliers used as detectors in laser-ranging systems have time

jitters ranging from 30 to 700 picoseconds (ps) at the single photoelectron level. Such photomultipliers also exhibit random gains on a pulse-by-pulse basis, which can cause uncertainties in the number of photocounts that occurred within the resolution time of the detector (Reference 9). Because the effects of stochastic detector transit times and gains have not been incorporated in more elaborate detector models to date, the photodetector is assumed to be ideal in the following analysis.

To derive the probability density functions of the foregoing Poisson process, it is assumed that the following axioms are valid:

- The probability of one photocount in an infinitesimal interval of width, Δt, is given by $P[1, \Delta t]$, where

$$\lim_{\Delta t \to 0} P[1, \Delta t] = \lambda(t)\,\Delta t \qquad (1)$$

- The probability of more than one photocount in the time interval, Δt, approaches zero as $\Delta t \to 0$

- The number of photocounts in any one interval is independent of those for all other disjoint intervals.

Given these axioms, the probability that the number of photocounts in interval (a, b) equals integer K is given by

$$P[K, (a, b)] = \left\{\exp\left[-\int_a^b \lambda(t)\,dt\right]\right\}\left[\int_a^b \lambda(t)\,dt\right]^K [K!]^{-1} \qquad (2)$$

where $\lambda(t) \geq 0$ is the time-varying expectation of the Poisson process.

For K = 0 and K = 1, equation 2 reduces to

$$P[0, (a, b)] = \exp\left\{-\int_a^b \lambda(t)\,dt\right\} \qquad (3)$$

$$P[1,(a,b)] = P[0,(a,b)] \cdot \int_a^b \lambda(t)\,dt \qquad (4)$$

Consider a realization of the process as shown in figure 1.

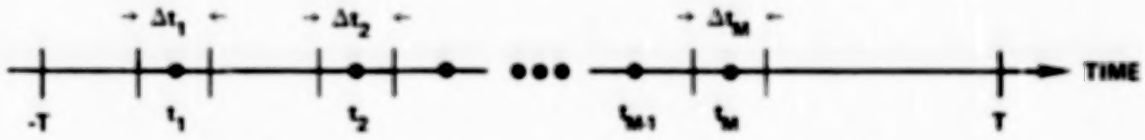

Figure 1. A possible realization of the random-point process.

Let $\{t_M\}$ denote the set of M numbers, $-T \leq t_1 < t_2 < \cdots < t_M \leq T$.

By first allowing infinitesimal intervals of width, Δt_j, about t_j, $j = 1, 2, \ldots, M$, the M dimensional-joint probability density function, $P(\{t_M\}, M)$, can be calculated as follows. By axiom 3 and equation 4, the probability that only one point will fall within each of these intervals with no counts outside of them is given by

$$\begin{aligned} P(\{t_M\}, M) \cdot [\Delta t_1 \cdot \Delta t_2 \cdot \ldots \cdot \Delta t_M] = {} & [P[0,(-T, t_1 - 1/2\,\Delta t_1)] \cdot \lambda(t_1)\,\Delta t_1] \\ & \cdot [P[0,(t_1 + 1/2\,\Delta t_1, t_2 - 1/2\,\Delta t_2)] \cdot \lambda(t_2)\,\Delta t_2] \\ & \cdot [P[0,(t_{m-1} + 1/2\,\Delta t_{m-1}, t_m - 1/2\,\Delta t_m)] \cdot \lambda(t_M)\,\Delta t_M] \\ & \vdots \\ & \cdot P[0,(t_M + 1/2\,\Delta t_M, T)] \end{aligned}$$

By equation 3, in the limit as $\Delta t_j \to 0$ for all j and $M \geq 1$,

$$P(\{t_M\}, M) = \exp\left\{-\int_{-T}^{T} \lambda(t)\,dt\right\} \prod_{j=1}^{M} \lambda(t_j) \qquad (5)$$

If no occurrences are observed, M = 0, $\{t_M\}$ is empty, and

$$P(\{t_o\}, 0) = P[0, (-T, T)] = e^{-Q} \tag{6}$$

where

$$Q = \int_{-T}^{T} \lambda(t)\, dt \tag{7}$$

Figure 2 illustrates the sample space of events for this random-point process. In figure 2,

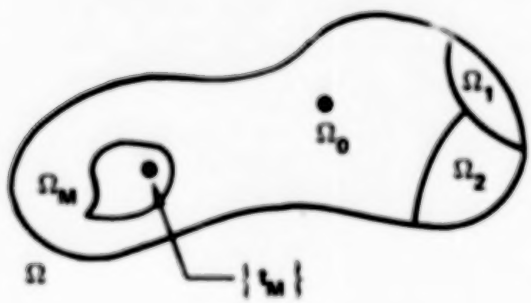

Figure 2. Sample space for the random-point process.

Ω_0 denotes the set of no occurrences in (-T, T); Ω_1, the set of one occurrence in (-T, T); Ω_M, the set of all possible sets of M events $\{t_M\}$; and Ω, the sure event (i.e., some number of points occurred at any instants in the interval (-T, T)).

As a special case, consider the process to be stationary with constant mean $\lambda(t) = \bar{K}$. Then all sample sequences of M occurrences within the interval, (-T, T), have the same likelihood, with joint probability density

$$P(\{t_M\}, M) = (\bar{K})^M \exp\{-2\bar{K}T\} \tag{8}$$

DERIVATION OF OPTIMUM ESTIMATORS

The mathematical forms of the MMSE and ML estimators are derived in this section, following methods previously outlined (References 3 and 4). These forms are shown to be equivalent for the case of Gaussian optical-pulse shapes and no background noise.

Minimum Mean-Square Error Estimators

For a given set of observed data, it is well-known that the conditional mean estimator minimizes the mean-square error of the estimate. However, to find the conditional mean estimator, the value of the optical-pulse delay, τ, must also be assumed to be a random variable. In addition, the prior density function of the delay, $P_\tau(\tau)$, must be known over the observation interval, (-T, T). This requirement can be severe for ranging receivers because often little is known about the statistical fluctuations in the range of the target. For example, in satellite laser ranging, the major purpose of the experiment is to gain just this statistical knowledge concerning the ranging station to satellite distance (Reference 1). Nonetheless, it is still instructive to derive the MMSE estimator, because its functional form can be given explicitly for cases that cannot be solved by the ML estimator, as the next section will show. For simplicity in the following derivations, the prior range density, $P_\tau(\tau)$, is assumed to be uniform over (-T, T), and the MMSE estimator is solved for rectangular, exponential, and Gaussian optical-pulse shapes.

As before, let τ denote the unknown range delay, and let $P_\tau(\tau)$ denote its prior probability density. Also, let t_j, $j = 1,2,\ldots,M$ denote the ordered instants of photoelectron emissions, and let $P(\{t_M\} \mid \tau)$ denote the conditional density of $\{t_M\}$, given τ. The MMSE estimator $\hat{\tau}$ is the conditional mean of the range, given the observed data, and can be written as

$$\hat{\tau} = P(\{t_M\}, M)^{-1} \int_{R_\tau} \tau P(\{t_M\} \mid \tau) P_\tau(\tau)\, d\tau \tag{9}$$

where

$$P(\{t_M\}, M) = \int_{R_\tau} P(\{t_M\} \mid \tau) P_\tau(\tau)\, d\tau \tag{10}$$

and R_τ = the observation interval.

Assuming Poisson statistics and $\lambda(t)$ for the optical pulse shape and using equations 5 through 7,

$$P(\{t_M\}|\tau) = \begin{cases} e^{-Q} \prod_{j=1}^{M} \lambda(t_j - \tau) & , M > 1 \\ 0 & , M = 0 \end{cases} \tag{11}$$

Substituting equations 10 and 11 into equation 9 yields

$$\hat{\tau} = \frac{\int_{R_\tau} \tau \left[\prod_{j=1}^{M} \lambda(t_j - \tau) \right] P_\tau(\tau)\, d\tau}{\int_{R_\tau} \left[\prod_{j=1}^{M} \lambda(t_j - \tau) \right] P_\tau(\tau)\, d\tau} \tag{12}$$

Note that, by this definition, $\hat{\tau}$ is undefined when no photoelectron emissions are observed. The equation 12 will be solved for rectangular, exponential, and Gaussian pulse shapes in the background free case.

Rectangular Pulse Shapes

Let the pulse shape be rectangular of width 2D, centered about zero. Then

$$\lambda(t) = \begin{cases} Q/2D \equiv \lambda_s & , |t| < D \\ 0 & , \text{otherwise} \end{cases} \tag{13}$$

and

$$P(\{t_M\}|\tau) = \begin{cases} e^{-Q} \lambda_s^M & , |t_j - \tau| \leq D, \text{ for all } j \leq M \\ 0 & , |t_j - \tau| > D \end{cases} \tag{14}$$

If the prior density of τ is uniform,

$$P_\tau(\tau) = \begin{cases} (2T)^{-1} & , |\tau| < T \\ 0 & , \text{otherwise} \end{cases} \tag{15}$$

Therefore,

$$P(\{t_M\}, M) = \int_{R_\tau} \frac{e^{-Q}\,\lambda s^M}{2T}\,d\tau = \frac{e^{-Q}\,\lambda s^M}{2T} \int_{R_\tau} d\tau \tag{16}$$

Figure 3 illustrates the method used to find R_τ, the range of the unknown delay value given $\{t_M\}$. Figure 3 shows that τ has the range, $[t_M - D, t_1 + D]$.

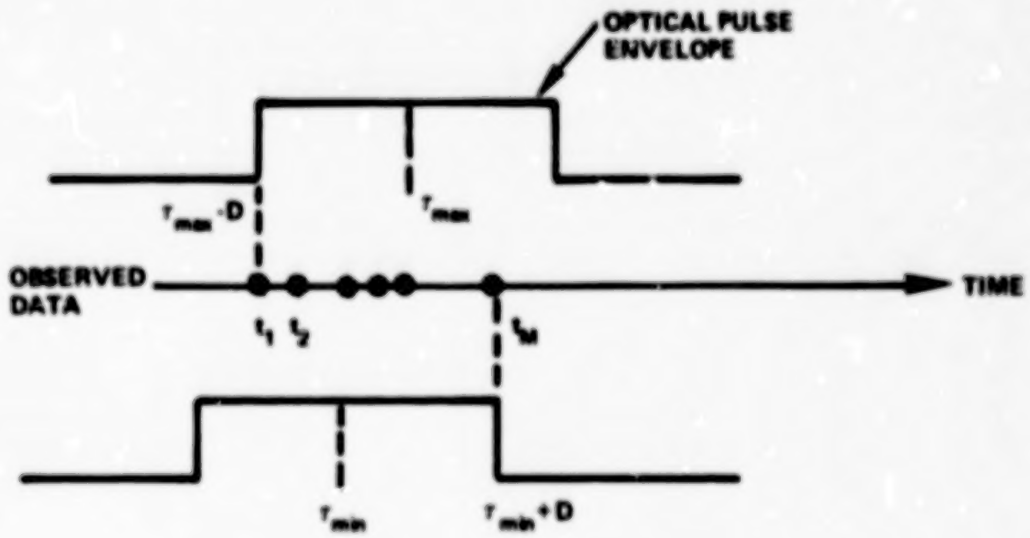

Figure 3. Prior range uncertainty limits given M photocount observations.

Using these limits for R_τ,

$$P(\{t_M\}, M) = \begin{cases} \dfrac{e^{-Q}\,\lambda_s^M}{2T}\,(2D + t_1 - t_M) & , M \geq 1,\ t_M - t_1 \leq 2D \\ 0 & , \text{otherwise} \end{cases} \tag{17}$$

For $M \geq 1$ and $t_M - t_1 \leq 2D$,

$$\int_{R_\tau} \tau\, P(\{t_M\} \mid \tau)\, P_\tau(\tau)\, d\tau = \frac{e^{-Q}\,\lambda_s^M}{2T}\left[\frac{(t_1 + t_M)}{2}(2D + t_1 - t_M)\right] \tag{18}$$

Substituting equations 17 and 18 into equation 9 yields, for rectangular pulses,

$$\hat{\tau}_{rect} = \frac{t_1 + t_M}{2} \tag{19}$$

which is valid for $M \geq 1$.

Exponential Pulse Shapes

Let the pulse shape be a decaying exponential with its origin at t = 0. Then,

$$\lambda(t) = \begin{cases} \dfrac{Q}{D}\exp(-t/D) & , t \geq 0 \\ 0 & , \text{otherwise} \end{cases} \tag{20}$$

Assuming that $t \geq 0$ and $M \geq 1$,

$$P(\{t_M\} \mid \tau) = e^{-Q} \prod_{j=1}^{M} \lambda(t_j - \tau) = e^{-Q}\,(Q/D)^M \prod_{j=1}^{M} e^{-(t_j - \tau)/D} \tag{21}$$

$$= e^{-Q}\,(Q/D)^M \exp\left(-\frac{M}{D}(\bar{t} - \tau)\right)$$

where

$$\bar{t} = (M)^{-1} \sum_{j=1}^{M} t_j$$

Substituting equations 20 and 15 into equation 10 yields

$$P(\{t_M\}, M) = e^{-Q}\left(\frac{Q}{D}\right)^M \frac{e^{-M\bar{t}/D}}{2T} \int_{R_\tau} e^{M\tau/D}\, d\tau \qquad (22)$$

From analysis similar to that shown in figure 3, the range of τ is found to be $[-T, t_1]$. Therefore, equation 22 can be evaluated as

$$P(\{t_M\}, M) = \alpha\left(\frac{D}{M}\right)\left[e^{Mt_1/D} - e^{-Mt/D}\right] \qquad (23)$$

where

$$\alpha = (Q/D)^M \exp(-Q - M\bar{t}/D)$$

Similarly, the numerator of equation 12 can be evaluated as

$$\alpha \int_{-T}^{t_1} \tau e^{M\tau/D}\, d\tau = \alpha\left[e^{Mt_1/D}\left(\frac{Dt_1}{M} - \frac{D^2}{M^2}\right) + e^{-MT/D}\left(\frac{DT}{M} - \frac{D^2}{M^2}\right)\right] \qquad (24)$$

Therefore, given $M \geq 1$, the optimum estimator for exponential pulse shapes is

$$\hat{\tau} = \frac{(t_1 - D/M)\, e^{Mt_1/D} + (T + D/M)\, e^{-MT/D}}{e^{Mt_1/D} - e^{-MT/D}} \qquad (25)$$

Note that, as for most cases of interest, $D \ll T$ and equation 25 simplifies to

$$\hat{\tau}_{exp} = (t_1 - D/M) \tag{26}$$

Bell-Shaped (Gaussian) Pulse Shapes

Let the optical pulse shape be Gaussian, centered at $t = 0$ with variance = D^2. Then,

$$\lambda(t) = \frac{Q}{\sqrt{2\pi}\, D}\, e^{-t^2/2D^2} \tag{27}$$

Assuming that $M \geq 1$,

$$\begin{aligned} P(\{t_M\} \mid \tau) &= e^{-Q}\left(\frac{Q}{\sqrt{2\pi}\, D}\right)^M \prod_{j=1}^{M} e^{-(t_j-\tau)^2/2D^2} \\ &= e^{-Q}\left(\frac{Q}{\sqrt{2\pi}\, D}\right)^M \exp\left\{-\frac{1}{2D^2}\sum_{j=1}^{M}(t_j-\tau)^2\right\} \end{aligned} \tag{28}$$

Substituting equations 28 and 15 into equation 10 yields

$$\begin{aligned} P(\{t_M\}, M) &= \int_{R_\tau} \frac{e^{-Q}}{2T}\left(\frac{Q}{\sqrt{2\pi}\, D}\right)^M \exp\left\{-\frac{1}{2D^2}\sum_{j=1}^{M}(t_j-\tau)^2\right\} d\tau \\ &= \beta \int_{R_\tau} \exp\left\{-\frac{1}{2D^2}\sum_{j=1}^{M}(t_j-\tau)^2\right\} d\tau \end{aligned} \tag{29}$$

where

$$\beta = \frac{e^{-Q}}{2T}\left(\frac{Q}{\sqrt{2\pi}\,D}\right)^{M} \text{, and } R_\tau = [-T, T]$$

Expanding the quadratic term in equation 29,

$$P(\{t_M\}, M) = \beta \int_{R_\tau} \exp\left[-\frac{1}{2D^2}(b - 2\tau c + M\tau^2)\right] d\tau \qquad (30)$$

where

$$b = \sum_{j=1}^{M} t_j^2 \text{ and } c = \sum_{j=1}^{M} t_j$$

Because $D \ll T$ for the case of interest, the area of the Gaussian pulse outside range (-T, T) is negligible. Therefore,

$$P(\{t_M\}, M) = \beta \int_{-\infty}^{\infty} \exp\left[\frac{1}{2D^2}(b - 2\tau c + M\tau^2)\right] d\tau \qquad (31)$$

which can be evaluated to yield (Reference 10)

$$P(\{t_M\}, M) = \beta \left[2\pi/M\right]^{1/2} \cdot D \cdot \exp\left\{\frac{c^2 - bM}{2D^2 M}\right\} \qquad (32)$$

In a similar fashion, the numerator of equation 12 becomes

$$\beta \int_{-\infty}^{\infty} \tau \exp\left[-\frac{1}{2D^2}(b - 2\tau c + M\tau^2)\right] d\tau$$

which can be evaluated as (Reference 11)

$$\beta (2\pi)^{1/2} (M)^{-3/2} \, c \, D \exp \left\{ \frac{c^2 - bM}{2D^2 M} \right\} \tag{33}$$

For $M \geq 1$, the ratio of equation 33 to equation 32 yields the optimum estimator for a Gaussian pulse,

$$\hat{\tau}_{GAUSS} = \frac{1}{M} \sum_{j=1}^{M} t_j \tag{34}$$

This estimator is simply the average of the observed emission times.

Maximum-Likelihood Estimator

When the prior distribution of ranges is completely unknown, an optimum estimator can still be formed by directly optimizing $P(\{t_M\}, M)$ for the observed photo-occurrence times, $\{t_M\}$. In this section, the ML estimator is derived, and its form is compared to the MMSE estimators derived in the previous section.

In general, let the time-varying expectation of the Poisson process depend on the parameter α so that

$$\lambda (t, \alpha) = S (t, \alpha) + \lambda_n \tag{35}$$

where λ_n represents a constant background count rate, and $S (t, \alpha)$ is the optical pulse shape, which is assumed to be known in both t and α. Here, α represents a general parameter. Using this form for $\lambda (t)$, equation 7 becomes

$$Q (\alpha) = \int_{-T}^{T} \lambda (t, \alpha) \, dt \tag{36}$$

and represents the average number of photocounts observed in interval (-T, T). The likelihood function of the M observed photocounts can be written as

$$P\left(\left\{t_M\right\}, M\right) = e^{-Q(\alpha)} \prod_{j=1}^{M} \left[S\left(t_j, \alpha\right) + \lambda_n\right] \tag{37}$$

The ML estimate of α is that value of α denoted as $\hat{\alpha}$, which maximizes equation 37. Because the logarithm is a monotone nondecreasing function of its parameter,

$$\hat{\alpha} = \mathrm{Max}_{\alpha} \left\{ \sum_{j=1}^{M} \ell n \left[S\left(t_j, \alpha\right) + \lambda_n\right] - Q\left(\alpha\right) \right\} \tag{38}$$

In general, a search procedure is required for finding $\hat{\alpha}$. However, if $S\left(t, \alpha\right)$ is piecewise differentiable, $\hat{\alpha}$ must satisfy

$$\frac{\partial}{\partial \alpha} \left\{ \sum_{j=1}^{M} \ell n \left[S\left(t_j, \alpha\right) + \lambda_n\right] - Q\left(\alpha\right) \right\} \Bigg|_{\alpha=\hat{\alpha}} = 0$$

which implies that

$$\frac{\partial}{\partial \alpha} Q\left(\alpha\right) \Bigg|_{\alpha=\hat{\alpha}} = \sum_{j=1}^{M} \left\{ \left(\frac{\partial}{\partial \alpha} S\left(t_j, \alpha\right) \right) \Big/ \left[S\left(t_j, \alpha\right) + \lambda_n\right] \right\} \Bigg|_{\alpha=\hat{\alpha}} \tag{39}$$

The ML estimate of α must satisfy equation 39 for the general estimation problem.

For ranging applications, the parameter, α, is delay time, τ, and the optical pulse shape can be written as $\lambda_s\left(t - \tau\right)$ as defined earlier. For this case, equation 38 becomes

$$\hat{\tau} = \mathrm{Max}_{\tau} \left\{ \sum_{j=1}^{M} \ell n \left[\lambda_s\left(t_j - \tau\right) + \lambda_n\right] - Q\left(\tau\right) \right\} \tag{40}$$

For most cases of interest, the signal pulse is well contained within the prior range uncertainty, which implies that the average photocount rate, Q, does not vary with delay time, τ. Therefore, if $\lambda(t)$ is once differentiable, the ML estimate of range delay, τ, must satisfy

$$\sum_{j=1}^{M} \left\{ \dot{\lambda}_s(t_j - \tau)/[\lambda_s(t_j - \tau) + \lambda_n] \right\} \Bigg|_{\tau=\hat{\tau}} = 0 \tag{41}$$

assuming the estimator has only one maximum.

For more general pulse shapes, the ML estimate, $\hat{\tau}$, can be found by maximizing the log likelihood ratio,

$$F(\tau) = \sum_{j=1}^{M} \ell n\,[\lambda_s(t_j - \tau) + \lambda_n] \tag{42}$$

with respect to τ. This distinction between differentiable and nondifferentiable pulse envelopes is important, because the error expression for the ML estimator can be found analytically for differentiable pulse envelopes only. For nondifferentiable pulses, other techniques are necessary for estimating the ranging receiver performance.

Comparison of Optimum Estimators

Table 1 summarizes the form of the optimum estimators of range delay for estimating MMSE and ML derived previously. In this section, the forms of these expressions will be examined with regard to their hardware implementation.

To directly implement the MMSE estimator expression for the Gaussian pulse, each photoelectron emission time must be observed and recorded, and the arithmetic mean must be computed. For nanosecond pulse-width lasers, this processing of the individual photooccurrence times is only possible with streak cameras or swept-image converters. Although such high-time resolution devices are now being used in laboratory applications, their relative complexity places this form of estimation at a disadvantage relative to other forms. In contrast, the expression for ML estimators for differentiable pulses can be readily implemented in two forms. By constructing the time functions,

$$q(t) = \dot{\lambda}_s(t)/[\lambda_s(t) + \lambda_n] \tag{43}$$

Table 1
Optimum Estimator Forms for Differentiable
and Nondifferentiable Pulse Envelopes

Pulse Type	MMSE	ML
Differentiable pulse envelopes	Gaussian: $\hat{\tau} = \frac{1}{M}\sum_{j=1}^{M} t_j$	General: $\sum_{j=1}^{M} \left\{ \dot{\lambda}_s(t_j - \tau)/\lambda_s(t_j - \tau) + \lambda_n \right\} \Big\|_{\tau = \hat{\tau}} = 0$ or: $\hat{\tau} = \mathrm{Max}_\tau \sum_{j=1}^{M} \left\{ \ell n \left[\lambda_s(t_j - \tau) + \lambda_n \right] \right\}$
Nondifferentiable pulse envelopes	Rectangular: $\hat{\tau} = (t_1 + t_M)/2$ Exponential: $\hat{\tau} = t_1 - D/M$	General: $\hat{\tau} = \mathrm{Max}_\tau \sum_{j=1}^{M} \left\{ \ell n \left[\lambda_s(t_j - \tau) + \lambda_n \right] \right\}$

and

$$v(t) = \ell n \left[\lambda_s(t) + \lambda_n \right]$$

either a correlation or a matched filter receiver can be constructed as shown in figures 4 and 5.

The instant when the output passes through zero (for q (t)) or a maximum (for v (t)) yields the estimate, $\hat{\tau}$. The start pulse to the time interval unit is usually derived from the transmitted laser pulse under extremely high signal conditions. Therefore, the range error introduced by the start channel is negligible in current system designs and will not be considered further here.

When such a system is operating with low signal-to-background ratios in the return signal path, several maxima or zero crossings can occur, yielding ambiguities in the location of the

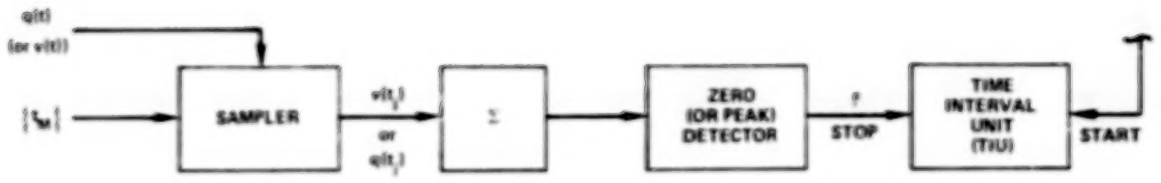

Figure 4. Correlation type ML receiver.

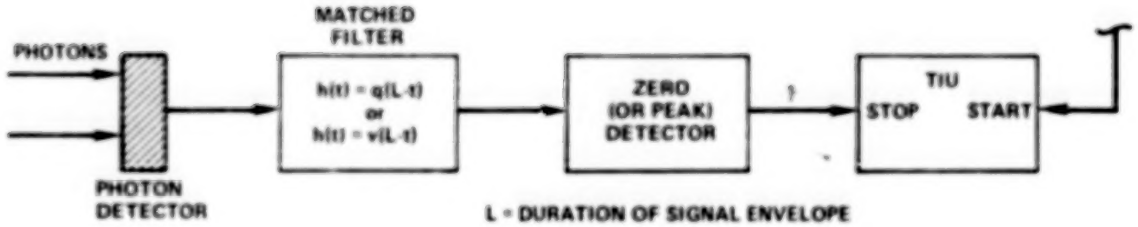

Figure 5. Matched-filter ML receiver.

range estimate. Under these conditions, the maxima that appears in the neighborhood of the densest photo-occurrences should be selected. An error in selecting this neighborhood can cause a ranging error much larger than an error in locating the occurrence time of the zero crossing or maximum. An expression for the probability of this event has been previously derived (Reference 3). Because of the relatively high signal-to-background count-rate ratio in current NASA ranging systems, this error should occur infrequently. However, for operating under less favorable ranging conditions, the increased probability of this event must be accounted for in the receiver design.

For rectangular and exponential pulse envelopes, the expressions for the optimum estimators are also directly implementable as shown in figures 6 and 7.

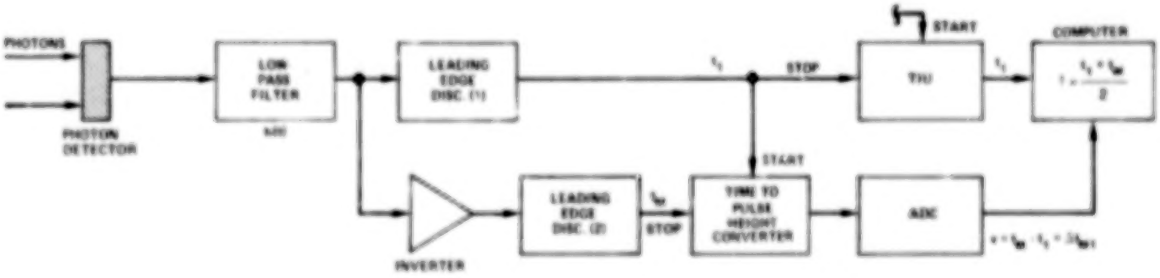

Figure 6. MMSE receiver for rectangular pulse envelopes.

For rectangular pulse envelopes, a low-pass filter is used following the photodetector. The impulse response, h (t), of this filter should be long enough to prevent its output voltage from returning to zero between successive photoevents within the duration of the optical pulse. The first discriminator will trigger on the leading edge of the filter output, which occurs at time t_1. The trailing edge of the filter output will trigger the second discriminator at time t_M. The threshold levels of both discriminators should be set high enough so that they do not trigger on the widely spaced single-photoelectron background counts. The output at time t_1 will stop the range-time interval counter, whereas the time between the first and last photoemissions will be measured and digitized by a time-to-pulse-height converter followed by the analog-to-digital converter. With these two measured quantities, a small minicomputer or microprocessor can easily compute tne correction to t_1 and form the optimum estimator, $\hat{\tau}$.

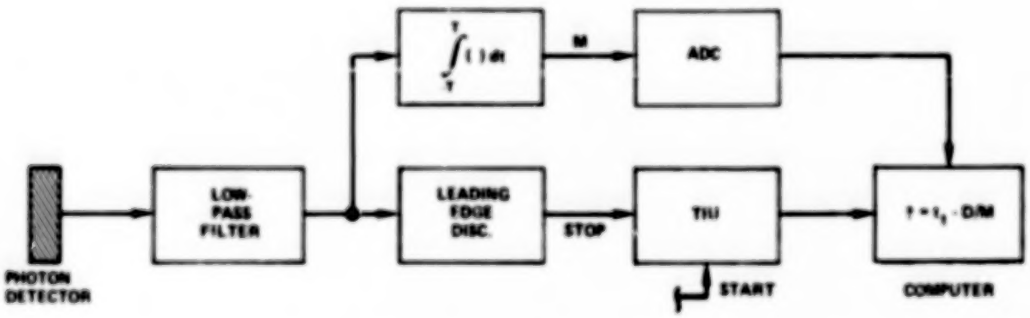

Figure 7. MMSE receiver for exponential pulse envelopes.

For exponential pulses, only one discriminator is used following the low-pass filter. Although the operation of this configuration is similar to that mentioned previously, the total number of photocounts, rather than t_M, is required as the second measurement. By passing the low-pass filter output through an integrator, its output at the end of the observation interval is directly proportional to M. This output is then digitized, and, as before, the computer can form the optimum estimator, $\hat{\tau}$.

A comparison of the four possible receiver implementations shows that, for receiver simplicity, one of the ML receivers should be chosen. Furthermore, it is currently more practical to implement the matched-filter type receiver than the correlation type, which requires a high-speed randomly triggered sampler unit. As was mentioned earlier, the matched filter can be constructed for one of two possible waveforms. For maximum flexibility with regard to input optical-pulse envelopes, it is evident from table 1 that the filter should be matched to v (t) and followed by a peak detector. This configuration is shown in figure 8, and its ranging performance is discussed in the following section.

A variation of this receiver, using a 50-percent rise time or constant-fraction discriminator in place of the peak detector is discussed in the section on "Performance of Suboptimum Receiver Strategies."

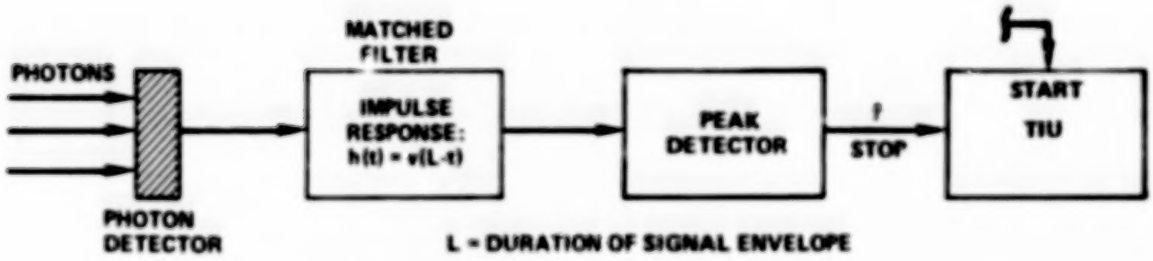

Figure 8. Implementable optimum ranging receiver configuration.

OPTIMUM AND SUBOPTIMUM ESTIMATOR PERFORMANCE

Because hardware considerations indicate that the ML form is the preferred optimum receiver, attention is first focused on deriving the error performance of this estimator. Although the following treatment closely resembles that of Bar-David (Reference 3) and gives only asymptotically valid results for differentiable pulse envelopes, it is nonetheless useful for a wide variety of pulse shapes encountered in practice. However, because the chosen hardware implementation is valid for general pulse shapes, results are cited that show the performance of this receiver used with rectangular and exponential pulses. Next, the results of a computer simulation of receiver performance are described. These results show how receiver performance changes when going from bell-shaped to rectangular optical pulse shapes, and when using leading-edge rather than peak detection following the matched filter. Finally, the ranging performance of these configurations is compared to that of a simple leading-edge receiver, which might be used when the optical-pulse shape is randomly broadened by the ranging target.

Variance of the ML Estimator

The variance of the estimate of delay, $\hat{\tau}$, can be approximated by expanding the log-likelihood ratio, $F(\hat{\tau})$, given in equation 42 at the true value of delay, τ_0. If the first two derivatives of $F(\tau)$ exist, equation 42 can be expanded in a Taylor series as

$$F(\tau) = F(\tau_0) + \dot{F}(\tau_0)(\tau - \tau_0) + \frac{\ddot{F}}{2!}(\tau_0)(\tau - \tau_0)^2 + \cdots \qquad (44)$$

Because the ML estimate is the value of τ that maximizes $F(\tau)$,

$$\frac{\partial}{\partial \tau} F(\tau)\Big|_{\tau=\hat{\tau}} = \dot{F}(\hat{\tau}) = 0 \tag{45}$$

Differentiating equation 44 with respect to τ, and using equation 45 yields

$$F(\hat{\tau}) = 0 = \dot{F}(\tau_0) + (\tau - \tau_0)\ddot{F}(\tau_0) + \cdots \tag{46}$$

from which it follows that the error in the estimate is

$$\epsilon_\tau = \hat{\tau} - \tau_0 = -\dot{F}(\tau_0)/\ddot{F}(\tau_0) \tag{47}$$

provided $\ddot{F}(\tau_0) \neq 0$. This constraint excludes strictly rectangular pulses from this analysis. Thus, the mean value and variance of the delay estimator error are

$$E[\epsilon_\tau] = -E[\dot{F}(\tau_0)/\ddot{F}(\tau_0)] \tag{48}$$

and

$$\mathrm{Var}[\epsilon_\tau] = E[(\dot{F}(\tau_0)/\ddot{F}(\tau_0))^2] - [E(\epsilon_\tau)]^2 \tag{49}$$

where $E[\ ]$ denotes the M-fold expectation over the set of random variables, $\{t_M\}$. By assuming $(E[\ddot{F}(\tau_0)])^2 >> \mathrm{Var}[\ddot{F}(\tau_0)]$, $\ddot{F}(\tau_0)$ can be replaced by its expected value in equations 48 and 49. Under this assumption,

$$E[\epsilon_\tau] = -E[\dot{F}(\tau_0)]/E[\ddot{F}(\tau_0)] \tag{50}$$

and

$$\begin{aligned}\mathrm{Var}[\epsilon_\tau] &= \left\{ E[(\dot{F}(\tau_0))^2] - E^2[\dot{F}(\tau_0)] \right\} / E^2[\ddot{F}(\tau_0)] \\ &= \mathrm{Var}\left\{ \dot{F}(\tau_0) \right\} / E^2\left\{ \ddot{F}(\tau_0) \right\}\end{aligned} \tag{51}$$

The characteristic functions of $\dot{F}(\tau_0)$ and $\ddot{F}(\tau_0)$ are

$$\text{Char}\,[\dot{F}(\tau_0)] = E\left[\exp\left\{ix\ \frac{\partial}{\partial\tau}F(\tau)\right\}\right]$$

$$= E\left[\exp\left\{ix\ \sum_{j=1}^{M}\dot{\lambda}_n(t_0-\tau_0)/\lambda_n(t_j-\tau_0)+\lambda_n)\right\}\right]$$

$$= E\left[\prod_{j=1}^{M}\exp\left\{ix\ \dot{\lambda}_n(t_j-\tau_0)/\lambda_n(t_j-\tau_0)+\lambda_n)\right\}\right]$$

and

$$\text{Char}\,[\ddot{F}(\tau_0)] = E\left[\exp\left\{ix\ \sum_{j=1}^{M}\frac{\partial}{\partial\tau}[\dot{\lambda}_n(t_j-\tau_0)/(\lambda_n(t_j-\tau_0)+\lambda_n)]\right\}\right] \qquad (52)$$

$$= E\left[\prod_{j=1}^{M}\exp\left\{ix\ \frac{\partial}{\partial\tau}\dot{\lambda}_n(t_j-\tau_0)/\lambda_n(t_j-\tau_0)+\lambda_n)\right\}\right] \qquad (53)$$

This can be evaluated by using Bar-David's results regarding expectation of product functions (Reference 3):

$$E\left[\prod_{j=1}^{M}f(t_j)\right] = e^{-Q}\ \sum_{m=0}^{\infty}([G(T)]^M/M!) = e^{-Q+G(T)} \qquad (54)$$

where

$$G(T) = \int_{-T}^{T} f(t)\,\lambda(t)\,dt \qquad (55)$$

Without loss of generality, the true delay, τ_0, can be set to zero, and, using equations 54 and 55,

$$\text{Char}\,[\dot{\hat{F}}(0)] = \exp\left\{ -Q + \int_{-T}^{T} \lambda(t) \exp\left\{ ix\, \frac{\dot{\lambda}(t)}{\lambda(t)} \right\} dt \right\} \tag{56}$$

Using the well-known property of characteristic functions,

$$E\,[\dot{\hat{F}}(0)] = -i \left\{ \frac{\partial}{\partial x} \text{Char}\,[\dot{\hat{F}}(0)] \right\} \Bigg|_{x=0}$$

$$= -i \left[\text{Char}\,[\dot{\hat{F}}(0)] \int_{-T}^{T} \lambda(t) \exp\left\{ ix\, \frac{\dot{\lambda}(t)}{\lambda(t)} \right\} i\, \frac{\dot{\lambda}(t)}{\lambda(t)}\, dt \right] \Bigg|_{x=0}$$

$$= \left[\text{Char}\,[\dot{\hat{F}}(0)] \Big|_{x=0} \right] \cdot \int_{-T}^{T} \dot{\lambda}(t)\, dt$$

Because equation 56 is equal to 1 when evaluated at x = 0,

$$E\,[\dot{\hat{F}}(0)] = \int_{-T}^{T} \dot{\lambda}(t)\, dt \tag{57}$$

Assuming that the pulse is well contained in (-T, T) implies that

$$\dot{\lambda}(\pm T) = \dot{\lambda}_s(\pm T) = \lambda_s(\pm T) = 0$$

which implies that

$$E\,[\dot{\hat{F}}(0)] = 0 \tag{58}$$

Thus, by equation 50, the ML estimator is unbiased.

Proceeding in a similar manner with the second derivative of F (τ),

$$\text{Char}\,[\ddot{\bar{F}}(0)] = \exp\left\{ - Q + \int_{-T}^{T} \lambda(t) \exp\left\{ ix\,\ddot{\bar{F}}(t) \right\} dt \right\} \tag{59}$$

To find the mean value of $\ddot{\bar{F}}$ (0),

$$E\,[\ddot{\bar{F}}(0)] = \left[\text{Char}\,[\ddot{\bar{F}}(0)]\Big|_{x=0} \right] \cdot \left[-i \frac{\partial}{\partial x} \int_{-T}^{T} \lambda(t) \exp\left\{ ix\,\ddot{\bar{F}}(t) \right\} dt \right]\Bigg|_{x=0}$$

$$= \int_{-T}^{T} \ddot{\bar{F}}(t)\,\lambda(t)\,dt = \int_{-T}^{T} \left[\ddot{\lambda}(t) - \frac{(\dot{\lambda}(t))^2}{\lambda(t)} \right] dt$$

which simplifies to

$$E\,[\ddot{\bar{F}}(0)] = - \int_{-T}^{T} \frac{(\dot{\lambda}(t))^2}{\lambda(t)}\,dt \tag{60}$$

To complete the calculations for Var (ϵ_τ),

$$\text{Var}\,[\dot{\bar{F}}(0)] = - \frac{\partial^2}{\partial x^2}\,\text{Char}\,[\dot{\bar{F}}(0)]\Big|_{x=0}$$

$$= [\text{Char}\,\dot{\bar{F}}(0)] \left\{ \int_{-T}^{T} [\dot{\bar{F}}(t)]^2\,\lambda(t) \exp\left\{ ix\,\dot{\bar{F}}(t) \right\} dt \right\}\Bigg|_{x=0}$$

Using equations 56 and 58, the foregoing expression simplifies to

$$\text{Var}\,[\dot{\bar{F}}(0)] = \int_{-T}^{T} \frac{[\dot{\lambda}(t)]^2}{\lambda(t)}\,dt = - E\,[\ddot{\bar{F}}(0)]$$

Finally, by using the definition of $\lambda(t)$,

$$\mathrm{Var}\,(\epsilon_\tau) = \left[\int_{-T}^{T} \frac{[\dot{\lambda}_s(t)]^2}{\lambda_s(t) + \lambda_n}\, dt \right]^{-1} \tag{61}$$

for the variance of the ML estimator timing error.

ML Estimator Error for Bell-Shaped Optical Pulses

As an application of these results, let the pulse shape be a raised cosine,

$$\lambda_s(t) = \begin{cases} \dfrac{Q}{D}\left(1 + \cos\left(\dfrac{2\pi t}{D}\right)\right), & \dfrac{-D}{2} < t < \dfrac{D}{2} \\ 0, & \text{otherwise} \end{cases} \tag{62}$$

where Q represents the average photoelectron level of the received optical pulse. This pulse shape closely approximates a Gaussian pulse shape, whose $\pm 3\sigma$ points lie at $\pm D/2$. The ML estimator variance for a ranging system using such a pulse shape is derived from equation 61:

$$\mathrm{Var}\,(\epsilon_\tau) = \frac{Q}{D}\left(\frac{2\pi}{D}\right)^2 \int_{-D/2}^{D/2} \frac{\sin^2(2\pi t/D)}{1 + \cos(2\pi t/D) + \dfrac{\lambda n}{Q}}\, dt$$

$$= \left[\frac{4\pi^2 Q}{D^2} \left(\frac{\lambda n}{Q} + 1 - \sqrt{\left(\frac{\lambda n}{Q} + 1\right)^2 - 1} \right) \right]^{-1} \tag{63}$$

$$= \frac{D^2}{4\pi^2}\left[\lambda n + Q - \sqrt{\lambda n\,(\lambda n + 2Q)}\right]^{-1}$$

where λ_n is the average number of background counts per pulsewidth, D. This result is well known and has been obtained by others (Reference 5). Note that, if the background noise is zero, the root-mean-square (rms) range error has the form

$$\sigma_r = D/[2\pi\sqrt{Q}\,] \tag{64}$$

where D is the full width of the optical pulse, and Q is the average number of photoelectrons per pulse.

ML Estimator Performance for Increasingly Rectangular Pulse Shapes

As shown earlier, the performance of the ML estimator cannot be found directly for systems using nondifferentiable optical pulse shapes. For practical systems, this does not present a fundamental problem because infinite bandwidth optical sources do not exist; therefore, all derivatives of real pulse shapes will be bounded. Nonetheless, because real pulse shapes are often more closely approximated by nondifferentiable envelopes than by differentiable ones, it is worthwhile to examine the ML estimator error performance of nondifferentiable pulse shapes.

It has been found that under conditions of no background with bell-shaped optical pulses, both ML and MMSE estimators asymptotically achieve the Cramer-Rao lower bound.* An expression for ML estimator performance was also found:

$$\mathrm{Var}\,[\epsilon_r \mid m \geq 1] = \frac{\sigma_p^2}{Q}\,\frac{Q e^{Q}}{1 - e^{Q}} \sum_{k=1}^{\infty} \frac{Q^k}{k \cdot k!} \tag{65}$$

which is based on at least one photoelectron occurrence. Here, σ_p represents the second moment of the pulse shape. As Q becomes large, given a raised cosine pulse shape, equation 65 reduces to equation 63, where λ_n is taken as zero.

To further investigate the ML estimator performance, a computer program was written that simulates the behavior of an ideal (i.e., ML) laser-ranging system. The critical assumption made by this program is that the time axis can be divided into a larger number of independent

*F. Davidson and L. Stephens, "Experimental Performance of Point Process Estimators of Optical Pulse Delay," to be published in IEEE Transactions in Communications, August 1978.

time bins, with the average photoelectron emission rate constant over any bin width. As the time bins shrink to zero width, the simulation results should approach the analytical results. Note that this assumption is consistent with that used in the section on "Mathematical Representation of a Poisson Process." The use of a finite number of time bins also corresponds to a receiver operating with a finite resolution time and, hence, finite bandwidth. Because this will always be the case in practice, this approximation was not believed to be restrictive.

The computer program first generates and stores the optical pulse shape of total energy, Q, at each time-bin value. Next, the matched-filter impulse response is generated and stored. Then, by considering each time bin independently, a random Poisson process was generated, with the mean value of the Poisson process at each time bin equal to the instantaneous optical intensity at the same bin. The random-count record was next convolved with the matched-filter impulse response to generate the log-likelihood expression of equation 42. Finally, the time estimate, $\hat{\tau}$, was chosen as the time bin at which the filter output was maximum. This process was repeated many times, while building a histogram of the time estimates, $\hat{\tau}$. Finally, the mean and standard deviations of the histogram were calculated. The mean value of the histogram, which represented the bias of the simulated ML estimator, was always near zero. The standard deviation represented the rms timing error for an ideal receiver operating at a given average photoelectron level, Q. By repeating the simulation program for different values of Q, the performance of the simulated receiver can be plotted as a function of average received photoelectrons per pulse. For programming simplicity, only background free cases were studied.

Figure 9 shows a representative plot of this process for a Gaussian pulse shape and an average signal level of 5 photoelectrons per pulse. The time resolution is 40 bins per pulse width and has the same scale for all plots. The count record and correlation function shown are those for the last (500th) count record, and the histogram is that for the stop times for the random Poisson process. The left most histogram bin is that for when no photoelectrons were generated in the random count record, and was not used in the calculation of the histogram moments.

Because a stop time was not estimated when no photoevents are recorded, the program computes the standard deviation of the timing error, given at least one photoelectron occurrence. As the width of the time bins shrink to zero, the simulation error results should equal those given in equation 65. For large Q, the simulation error results should also equal equation 61, but discrepancies will exist for small Q values because the approximations used to obtain equation 61 preclude the case of small Q.

For program validation, the average number of photocounts after each simulation run was compared to the Q value used in the program. In each case, the average number computed by the program differed by less than 1 percent from Q. As a second check, the simulated performance of a system using the raised cosine pulse defined in equation 62 was compared

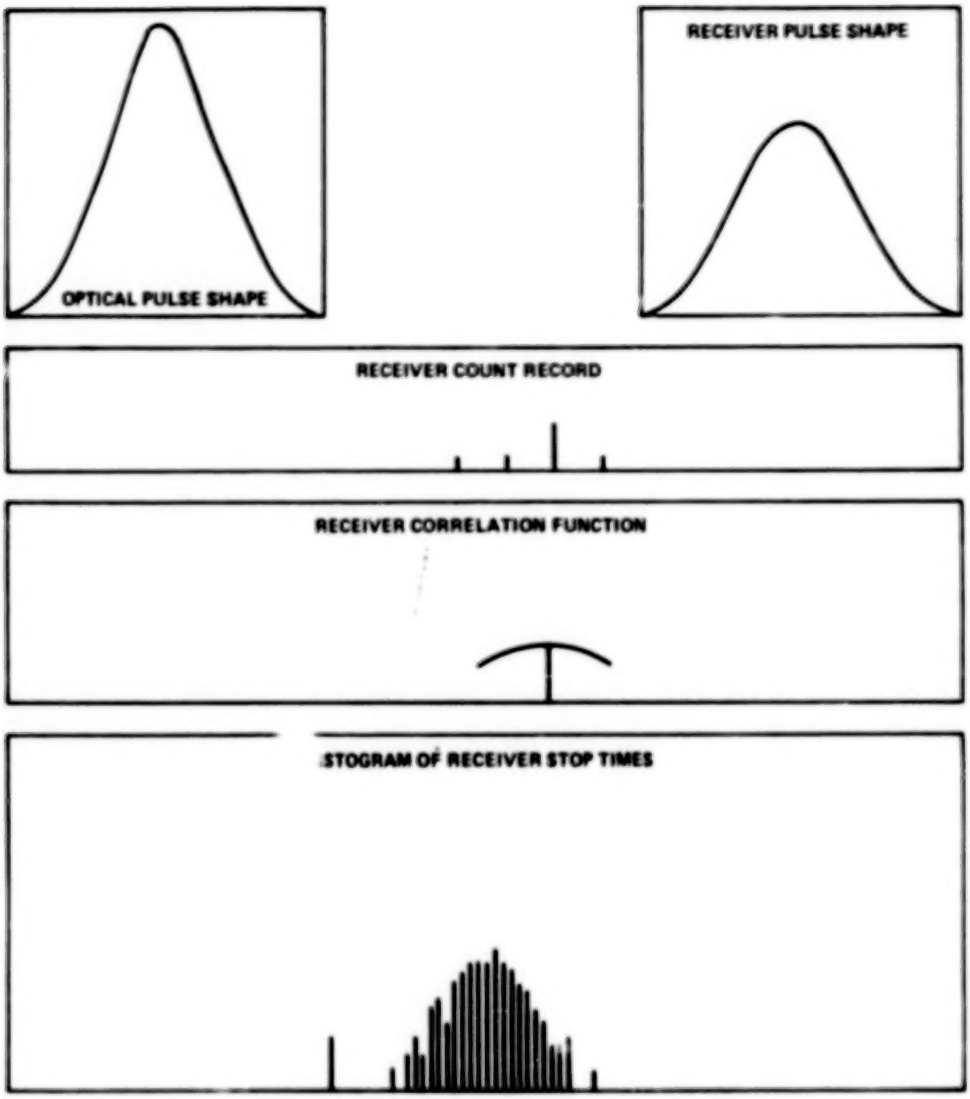

Figure 9. Representative simulation results for Q = 5 and Gaussian pulse shape.

to the analytical results predicted by equation 65 in the range from 1 to 100 photoelectrons. Shown in figure 10, these results indicate excellent agreement between analytical and simulated receiver performance. For all further simulations, a time resolution of 40 bins per pulse duration and 500 counts per histogram were also used.

Figure 11 shows simulation results for the ML receiver operating with a Gaussian pulse of standard deviation, σ_p = D/6. For comparison, the simulated performance of a raised cosine with a full width of D is also shown. Figure 11 illustrates the nearly equal timing resolution obtainable with these two bell-shaped pulses.

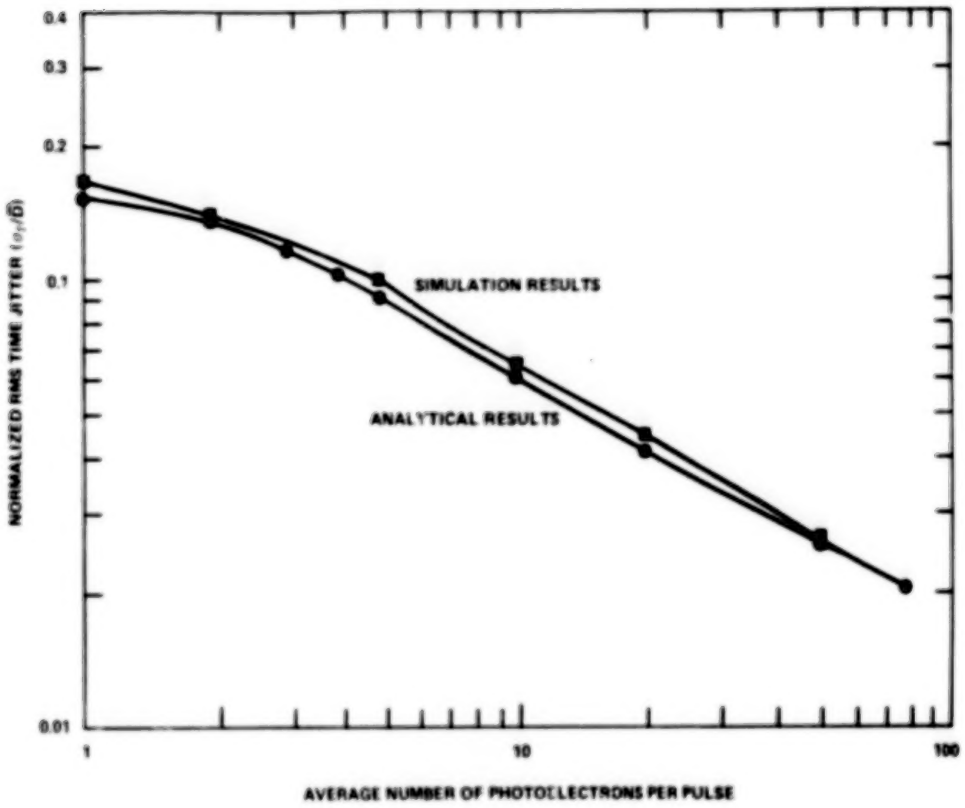

Figure 10. Comparison of analytical and simulated ML performance for raised-cosine optical-pulse shape, given at least one photoelectron observation and no background counts.

To investigate the ML receiver performance with rectangular pulse shapes, the raised-cosine pulse shape was raised to a fractional power, F. In the limit, as F approaches zero, the pulse shape approaches a rectangle. Further simulations were carried out for F values of 0.5, 0.1, and 0.01. Figure 12 shows the resulting optical-pulse shapes, and figure 13 shows the performance of the receiver. These curves, which represent new results in this area, show how the slopes of the rms time-jitter curve changes from $\alpha_1/\sqrt{Q}$ for bell-shaped pulses, to α_2/Q for rectangular pulses, where α_1 and α_2 are constants. The curve for F = 0.01 is in good agreement with

$$\frac{\sigma_\tau}{D} = \frac{\sqrt{\mathrm{Var}\left\{\epsilon_\tau/m \geq 1\right\}}}{D} = Q^{-1}\left[\frac{(1 - e^{-Q} - Q\,e^{-Q} - Q^2\,e^{-Q}/2)}{2\,(1 - e^{-Q})}\right]^{1/2} \qquad (66)$$

which is the expression calculated by Bar-David for the MMSE timing error when using a rectangular optical pulse (Reference 4).

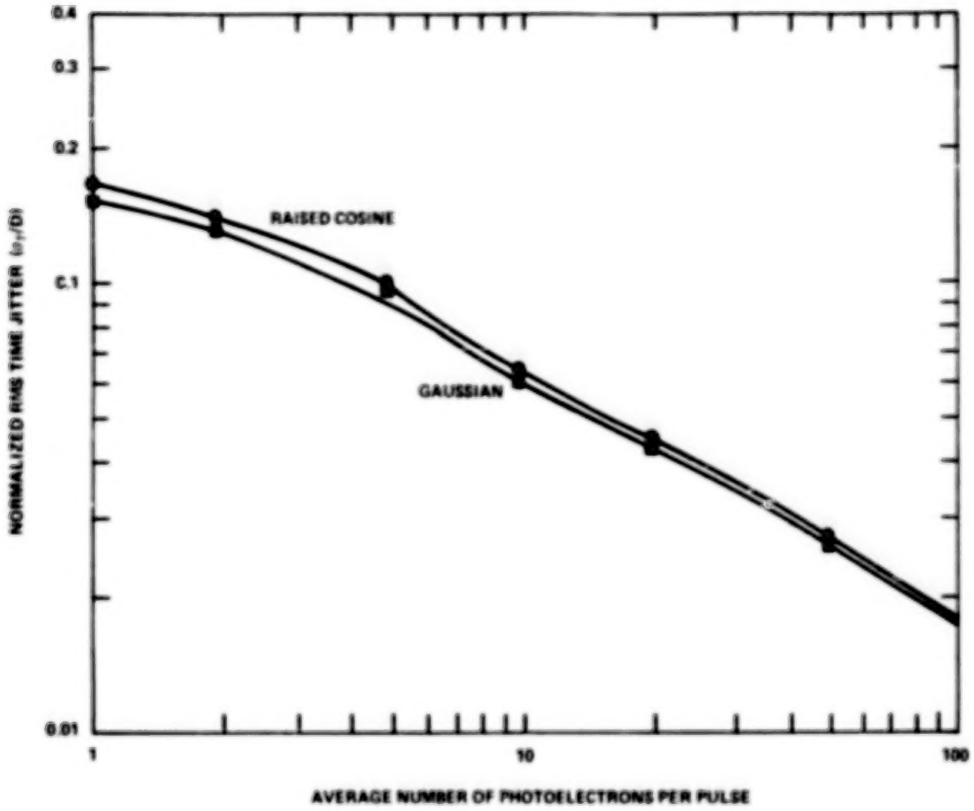

Figure 11. Comparison of simulated ML performance for raised-cosine and Gaussian optical-pulse shapes, given at least one photoelectron observation and no background counts.

It is evident from figure 13 that, to minimize ranging error, a bell-shaped optical pulse shape should be chosen for operating with average signals of less than 15 photoelectrons per pulse and that a rectangular pulse should be chosen for operating at higher signal levels. The more rapid decrease of ranging error versus received photoelectron level should strongly motivate the use of sharp leading- and trailing-edged pulses when possible in pulsed laser ranging systems.

PERFORMANCE OF SUBOPTIMUM RECEIVER STRATEGIES

Several studies have been made of suboptimal ranging-receiver configurations, including systems using a high-resolution leading-edge receiver (References 6 and 7). One stated advantage of this and other proposed leading-edge strategies is that they are simplier to implement than the ML receiver. Another possible advantage is that electronics are currently suited to their implementation or that the strategies can be used when the optical-pulse shape is not known in advance, as is the case for satellite-induced signal broadening (Reference 12). In this section, the performance characteristics of two possible leading-edge receivers are discussed.

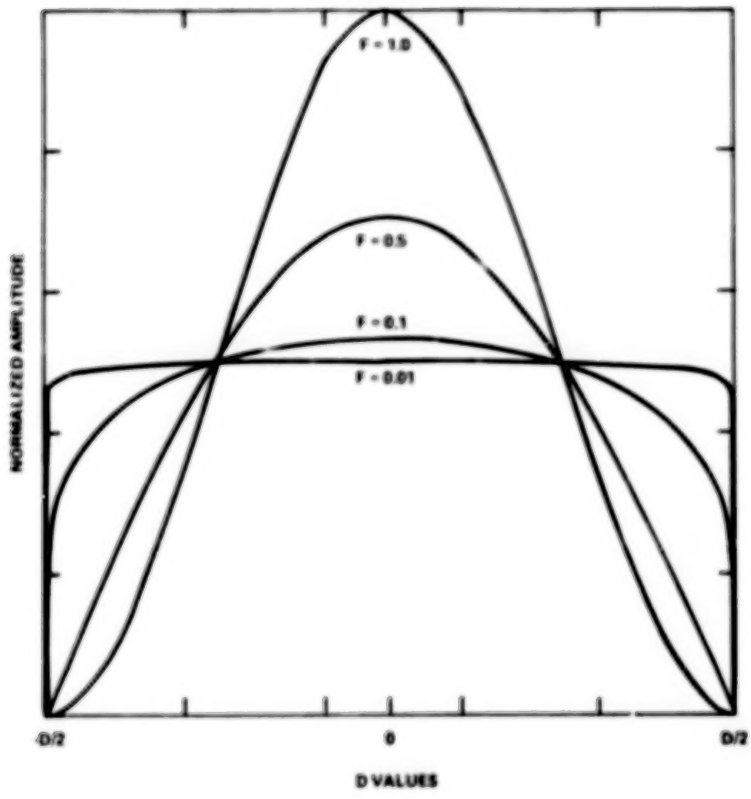

Figure 12. Pulse shapes used to investigate ML-receiver performance changes from bell-shaped to rectangular optical pulses.

Figure 14 shows the performance of a high time-resolution leading-edge receiver when the receiver is operating with a 400-ps rectangular optical pulse. For comparison, figure 14 also shows the simulated performance of an ML receiver operating with a nearly identical pulse shape (F = 0.01 curve of figure 12). The receiver model for the leading-edge receiver assumed a 5-ps time resolution with the trigger threshold set at the 2-photoelectron level. Such a receiver can be implemented by doing numerical calculations on the digitized output data from a circularly swept image-converter tube. Two such image-converter receiver systems are being developed at the Goddard Space Flight Center.

The performance of this receiver was also analyzed assuming nonideal image-converter gains. A gamma distribution was assumed for the pulse-height distribution of the swept-image tube, and the receiver performance was calculated for different values of the normalized variance of the gamma distribution. Figure 14 shows two performance curves for the normalized variance values of the gamma distribution of 1 and 1/3. In the signal region shown, the nonideal pulse-height resolution is shown to increase receiver errors only slightly. As is readily apparent in the figure, use of such a leading-edge receiver should be justified only under the condition of large return-pulse shape uncertainties. When the pulse shape is

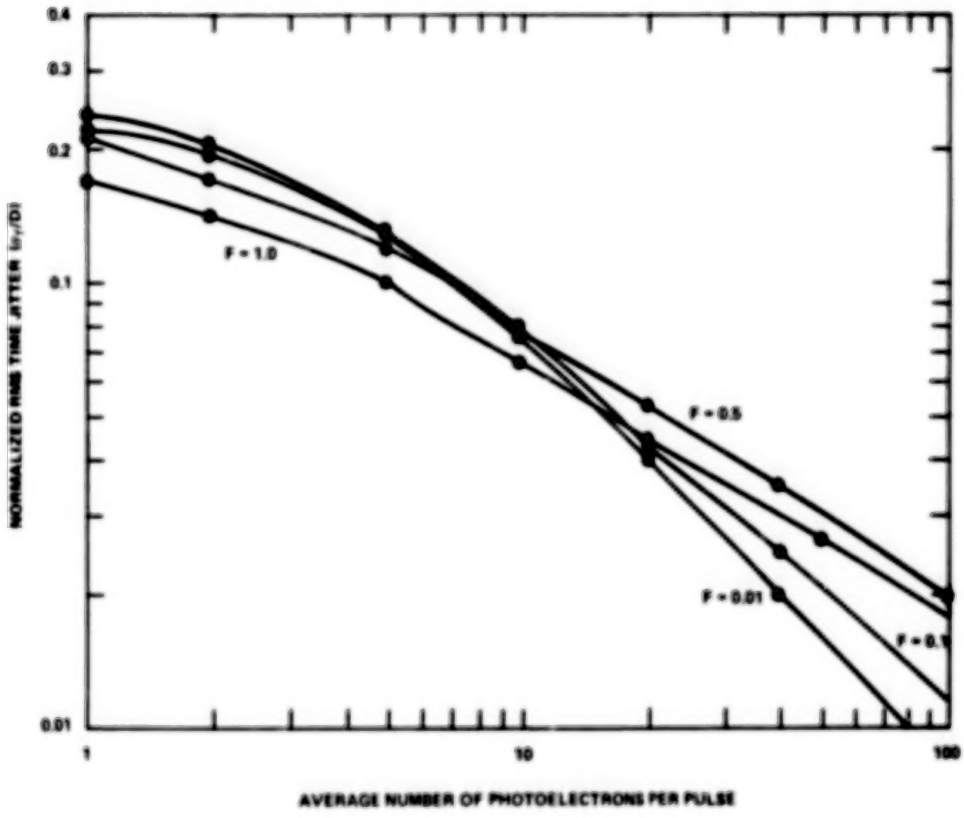

Figure 13. ML-receiver performance for increasingly rectangular optical-pulse shapes.

known in advance, such a leading-edge receiver requires approximately 10 times more return-pulse energy than an ML receiver to achieve the same ranging performance.

Figure 15 shows the performance of several matched-filter type receivers for a raised-cosine optical-pulse shape. The mismatched ML receiver represents a filter matched to the pulse shape rather than to the logarithm of the pulse shape. The leading edge receivers have filters followed by a discriminator with triggers on the 50-percent risetime point of the filter output waveform. The advantage of this type receiver is that such discriminators have been in use for many years in both nuclear research and are used in current laser ranging systems (Reference 1). The use of such discriminators following a matched-filter degrades receiver error performance only slightly in the signal region shown.

The similar performance of the matched-filter and mismatched ML receivers in figure 15 suggest that this type of receiver structure is relatively insensitive to small optical-pulse shape variation. Furthermore, the similar error performance of 50 percent versus peak detection also suggests that the exact trigger point as a fraction of the total pulse height is not critical if the trigger fraction does not change from one received laser pulse to the next.

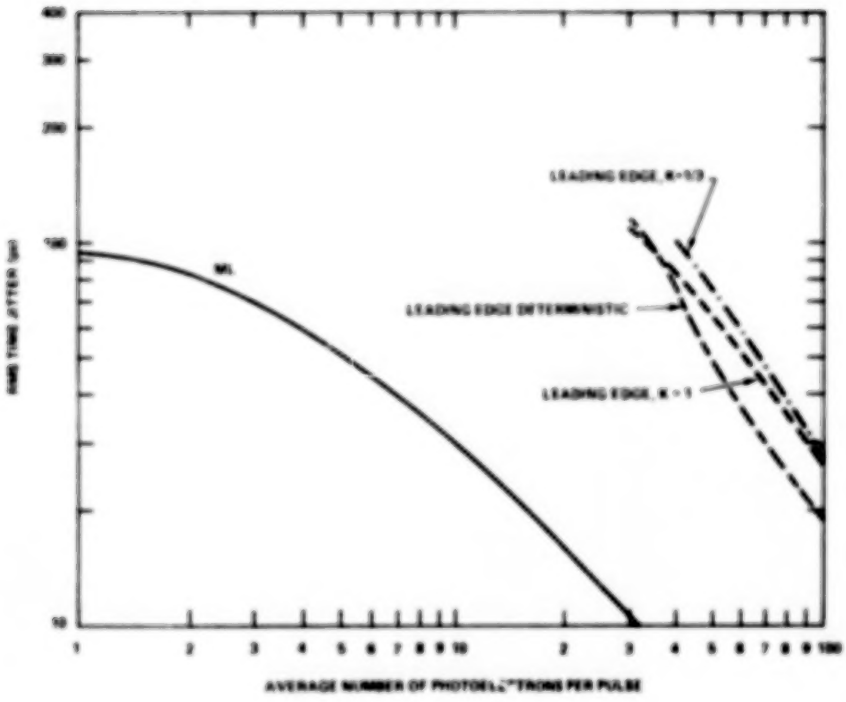

Figure 14. ML and high-resolution leading-edge receiver performance for 400-ps rectangular optical-pulse shapes. Leading-edge deterministic represents deterministic receiver gain, and K is the normalized variance of stochastic receiver gains.

However, both leading-edge receivers have a signal-energy-dependent time bias, that was not present when using peak detection following the matched-filter. This bias consists of a constant bias that is nominally equal to one-fourth of the filter impulse response full width plus a small signal-dependent term. Figure 16 is a plot of this small term. Although the constant term of the bias can be removed at any time during operation of the ranging receiver, the signal-dependent term could cause significant errors when the desired range resolution is a small fraction of the optical-pulse width. By measuring the total number of electrons received per pulse, this smaller signal-dependent bias term can be removed on a pulse-by-pulse basis, but only at the expense of additional receiver complexity. Although this receiver configuration is desirable from the viewpoint of range-error performance, these potential bias errors might limit the use of constant-fraction discriminators following the receiver filter.

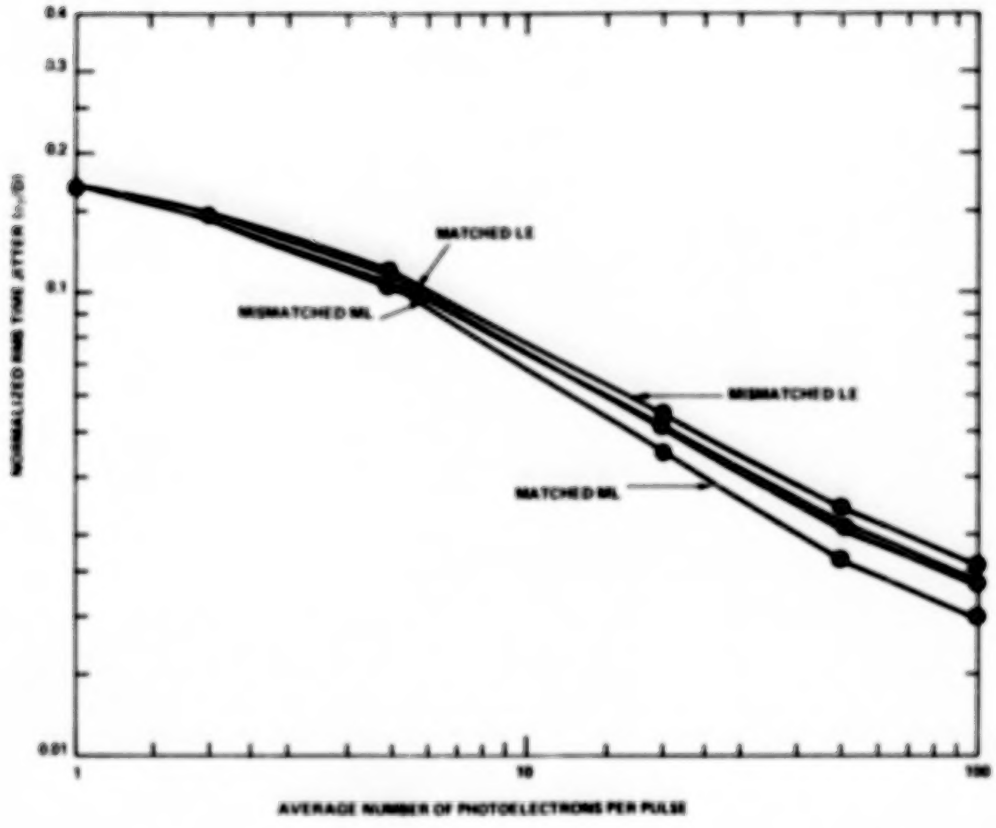

Figure 15. Performance of several matched-filter type receivers to bell-shaped optical pulses, given at least one photoelectron observation. Mismatched filters represent filter impulse responses equal to the laser pulse shape rather than to the logarithm of the pulse shape. LE represents timing to the 50-percent point on the leading edge of the filter output waveform; the ML receivers time to the peak of the waveform.

CONCLUSIONS AND AREAS FOR FUTURE STUDY

This document has summarized previously proposed methods for optimum direct-detection laser-ranging receivers and has compared the performance of these candidate receiver implementations by using computer simulations of the detection process. The ML and MMSE estimators were found to give the same performance for both bell-shaped and rectangular optical-pulse shapes when no background radiation existed. Of several hardware receiver implementations presented, the matched-filter peak-detector was found to be preferable from the standpoint of optimum performance and receiver simplicity. Although electronics are available for using a constant-fraction discriminator following the matched-filter, a signal-level-dependent time bias exists with this implementation. To achieve accuracies to a small fraction of the optical-pulse width, this bias, which can be compensated for on a pulse-by-pulse basis, must be addressed in the receiver design.

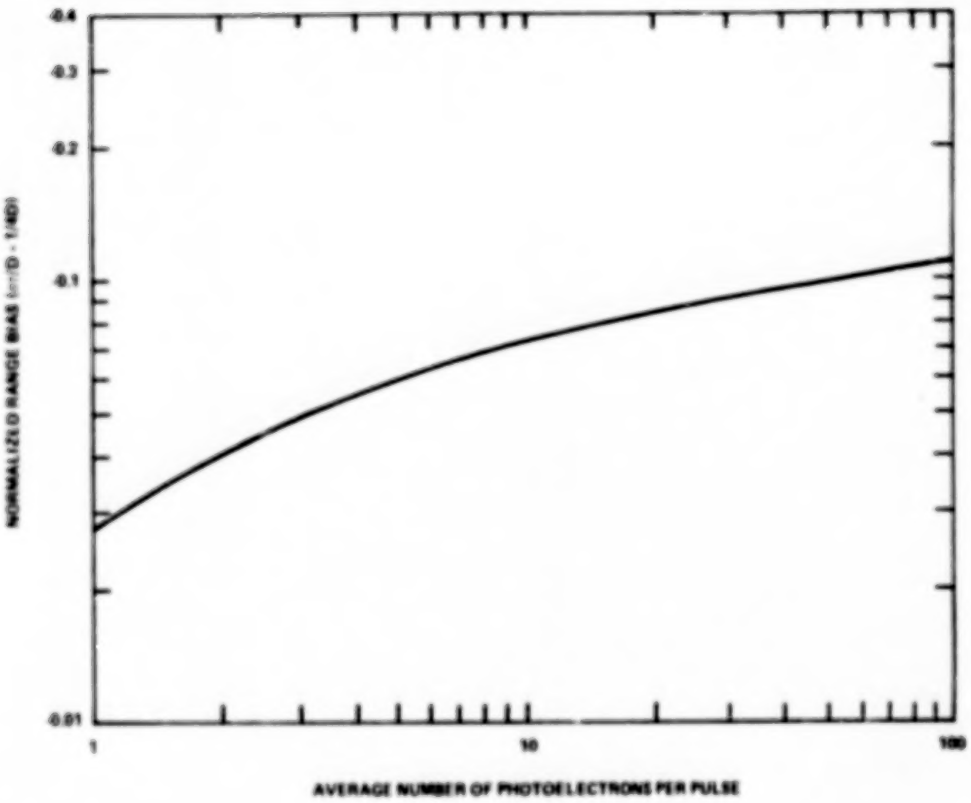

Figure 16. Signal-dependent range bias when using a matched filter followed by a 50-percent risetime discriminator. For symmetrical optical-pulse shapes, the static range bias is nominally 1/4D. Note that, for large numbers of photoelectrons per pulse, the range bias can be large compared to the random range errors about this value.

Several areas should be investigated further to fully characterize the ranging performance of the receiver configurations addressed in this study. Throughout this document, the receiver processing electronics were assumed to have access to the individual photo-occurrence times. In turn, these occurrence times were assumed to be unit amplitude delta functions in time. In reality, the outputs of the best available optical detectors have both stochastic gains and stochastic transit times. These random factors will further degrade the receiver performance from those reported in this document. A more elaborate detection model could take these additional receiver uncertainties into account. Further computer simulation work might also yield insight into the operation of matched-filter type receivers under nonzero background conditions and when using constant-fraction discriminators with sharp-edged optical pulses. Detection and false-alarm probabilities, which have not been addressed here, must be studied for implementable receiver strategies.

Supporting experimental data, especially that with carefully measured average signal levels, would be valuable to laser-ranging system designers. Using these data with the analytical and simulation studies would not only serve to quantify the range error attributable to each

ranging receiver component, but also would lay the required groundwork for much improved laser-ranging system performance.

ACKNOWLEDGMENTS

The author gratefully acknowledges the guidance of Dr. Lee Davisson and Dr. Michael Fitzmaurice and the many helpful discussions with Dr. Ramakrishna Iyer.

Goddard Space Flight Center
National Aeronautics and Space Administration
Greenbelt, Maryland June 1978

Blank Page

REFERENCES

1. Fitzmaurice, M. W., "Ground-Based and Space-Based Laser Ranging Systems," NASA Technical Paper 1149, January 1978.

2. Goodman, J. W., "Comparative Performance of Optical-Radar Detection Techniques," *IEEE Trans. Aerospace and Electronic Systems,* **AE2** (5), September 1966, p. 526.

3. Bar-David, I., "Communication Under the Poisson Regime," *IEEE Trans. Information Theory,* **IT-15** (1), January 1969, p. 31.

4. Bar-David, I., "Minimum-Mean-Square-Error Estimation of Photon Pulse Delay," *IEEE Trans. Information Theory,* **IT-21**, May 1975, p. 326.

5. Lee, G., and G. Schroeder, "Optical Pulse Timing Resolution," *IEEE Trans. Information Theory,* **IT-22**, January 1976, p. 114.

6. Iyer, R. S., "Threshold Detection in Pulsed Laser Ranging," *Applied Optics,* **15** (6), June 1976, p. 1349.

7. Iyer, R. S., "Arrival Times of Satellite-Broadened Laser Pulses," *IEEE Trans. Aerospace and Electronic Systems,* **AES-12** (5), September 1976, p. 577.

8. Mandel, L., "Phenomenological Theory of Laser Beam Fluctuations and Beam Mixing," *Physical Review,* **138** (3B), May 1965, p. B753.

9. Abshire, J., and H. Rowe, "Characterization of Gigahertz Bandwidth Photomultipliers," NASA TM-78028, December 1977.

10. Gradshteyn, I. S., and I. M. Ryzhik, *Table of Integrals, Series, and Products,* Academic Press, New York, 1965, p. 307.

11. Gradshteyn, I. S., and I. M. Ryzhik, *Table of Integrals, Series, and Products,* Academic Press, New York, 1965, p. 337.

12. Fitzmaurice, M. W., P. O. Minott, J. B. Abshire, and H. E. Rowe, "Prelaunch Testing of the Laser Geodynamic Satellite (LAGEOS)," NASA Technical Paper 1062, October 1977.

1. Report No. NASA TP-1315	2. Government Accession No.	3. Recipient's Catalog No.
4. Title and Subtitle A Comparative Study of Optimum and Suboptimum Direct-Detection Laser Ranging Receivers		5. Report Date September 1978 6. Performing Organization Code 723
7. Author(s) James B. Abshire		8. Performing Organization Report No. G-7802-F15
9. Performing Organization Name and Address Goddard Space Flight Center Greenbelt, Maryland 20771		10. Work Unit No. 506-18-26 11. Contract or Grant No.
12. Sponsoring Agency Name and Address National Aeronautics and Space Administration Washington, D.C. 20546		13. Type of Report and Period Covered Technical Paper 14. Sponsoring Agency Code
15. Supplementary Notes		

16. Abstract

A summary of previously proposed receiver strategies for direct-detection laser ranging receivers is presented. Computer simulations are used to compare performance of candidate implementation strategies in the 1- to 100-photoelectron region. Under the condition of no background radiation, the maximum-likelihood (ML) and minimum mean-square error (MMSE) estimators were found to give the same performance for both bell-shaped and rectangular optical-pulse shapes. For signal energies greater than 10 photoelectrons, the root-mean-square (rms) range error is shown to decrease as $Q^{-1/2}$ for bell-shaped pulses and Q^{-1} for rectangular pulses, where Q represents the average pulse energy. Of several receiver implementations presented, the matched-filter peak detector was found to be preferable. A similar configuration, using a constant-fraction discriminator, exhibited a signal-level dependent time bias. Suggestions for future study are also included.

17. Key Words (Selected by Author(s))	18. Distribution Statement
Laser radar, Laser ranging systems, Direct-detection receiver, Radar performance	STAR Category 36 Unclassified–Unlimited

19. Security Classif. (of this report)	20. Security Classif. (of this page)	21. No. of Pages	22. Price*
Unclassified	Unclassified	44	$4.50

* For sale by the National Technical Information Service, Springfield, Virginia 22161

FC 25-44 (10/77)

NASA-Langley, 1978

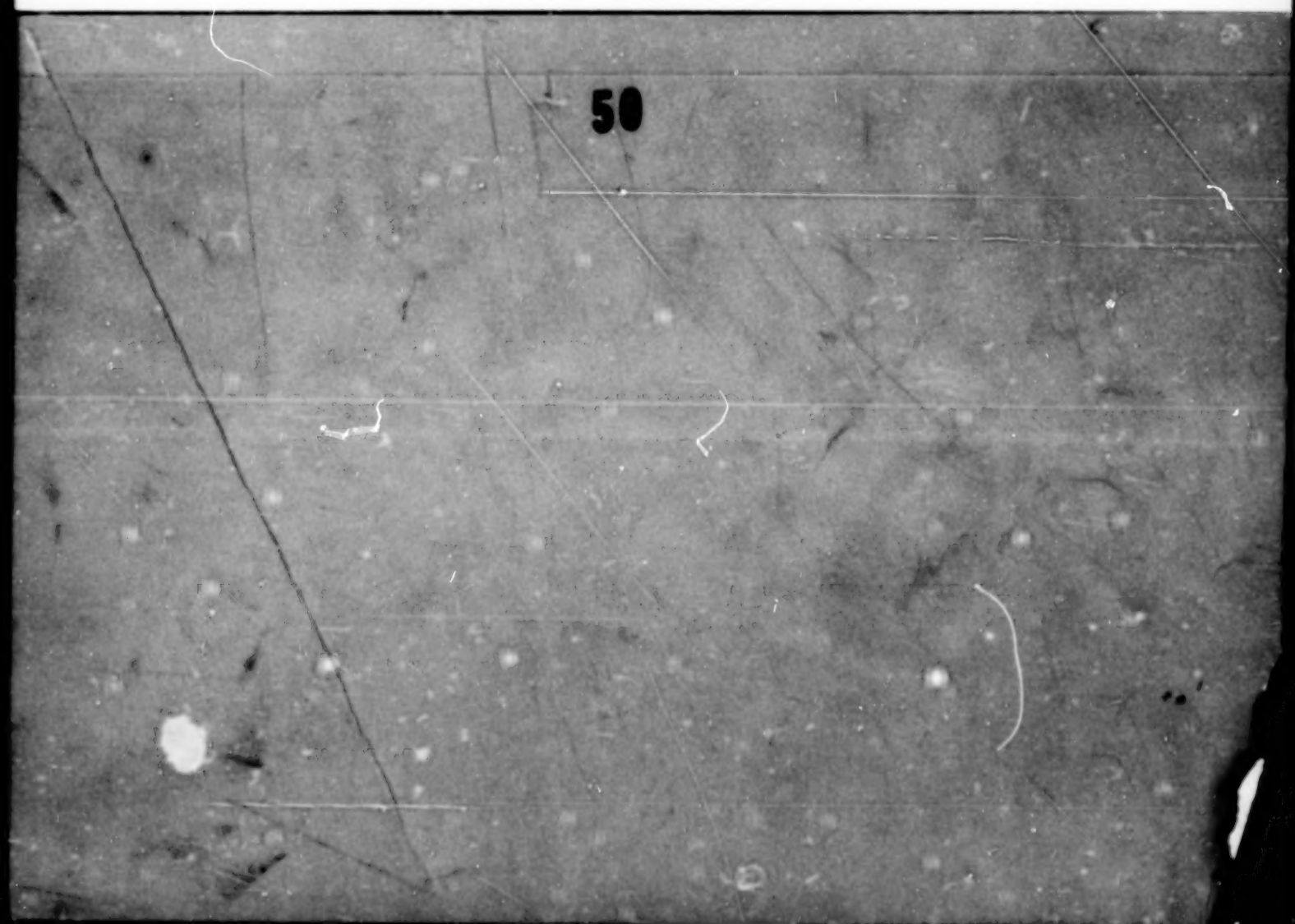
50

END

MAR 16 1979